Mon. Not. R. Astron. Soc. **372,** 1217–1226 (2006) doi:10.1111/j.1365-2966.2006.10923.x

A photon breeding mechanism for the high-energy emission of relativistic jets

Boris E. Stern[1,2,3]★ and Juri Poutanen[3]★

[1]*Institute for Nuclear Research, Russian Academy of Sciences, Prospect 60-letija Oktjabrja 7a, Moscow 117312, Russia*
[2]*Astro Space Centre, Lebedev Physical Institute, Profsoyuznaya 84/32, Moscow 117997, Russia*
[3]*Astronomy Division, PO Box 3000, FIN-90014 University of Oulu, Finland*

Accepted 2006 August 8. Received 2006 July 26; in original form 2005 September 15

ABSTRACT

We propose a straightforward and efficient mechanism for the high-energy emission of relativistic astrophysical jets associated with an exchange of interacting high-energy photons between the jet and the external environment. Physical processes playing the main role in this mechanism are electron–positron pair production by photons and the inverse-Compton scattering. This scenario has been studied analytically as well as with numerical simulations demonstrating that a relativistic jet (with the Lorentz factor larger than 3–4) moving through the sufficiently dense, soft radiation field inevitably undergoes transformation into a luminous state. The process has a supercritical character: the high-energy photons breed exponentially being fed directly by the bulk kinetic energy of the jet. Eventually particles feedback on the fluid dynamics and the jet partially decelerates. As a result, a significant fraction (at least 20 per cent) of the jet kinetic energy is converted into radiation mainly in the MeV–GeV energy range. The mechanism maybe responsible for the bulk of the emission of relativistic jets in active galactic nuclei, microquasars and gamma-ray bursts.

Key words: acceleration of particles – instabilities – radiation mechanisms: non-thermal – shock waves – methods: numerical – galaxies: active – gamma-rays: bursts.

1 INTRODUCTION

Traditionally, the dissipation of a relativistic bulk motion into radiation is assumed to be associated with the shock acceleration of charged particles. In a relativistic case, its role is limited by a number of factors (see e.g. Bednarz & Ostrowski 1999; Achterberg et al. 2001). Derishev et al. (2003) and Stern (2003) independently suggested that interacting *neutral* particles can convert bulk kinetic energy into radiation much more efficiently than this can be done by charge particles. Indeed, the neutral particles easily cross the shock front or the boundary of the shear layer in both directions and can be converted into charged particles for example via $e^{\pm}$ pair productions by two photons. Pairs in turn convert their energy into photons by Compton scattering, some of which cross the boundary again. Such exchange of particles between media moving with respect to each other with high Lorentz factor works in the same way as Fermi acceleration, but more efficiently as there is no problem with diffusion through the boundary layer. This process can proceed in a runaway manner where the high-energy photons breed exponentially similar to neutron breeding in nuclear chain reaction.

Stern (2003) demonstrated with numerical simulations that in the case of an ultrarelativistic shock in a moderately dense medium (above $\sim 10^4$ particles cm^{-3}) this process leads to a dramatic increase in the shock high-energy emission (electromagnetic catastrophe) and eventually to the elimination of the shock front, which is converted into a smooth radiation front. Such effect can take place in gamma-ray bursts. In this work, we consider the same scenario for a different kind of relativistic fluid: a shear flow in astrophysical jets. While we specifically consider here jets in active galactic nuclei (AGNs) which emit tremendous power in form of the gamma-rays in the MeV–TeV energy range, the mechanism can operate in the jets from microquasars as well as in gamma-ray bursts.

There exist different models of the jet emission mechanism, probably the most popular one is associated with internal shocks in the jet (Rees 1978; Paczyński & Xu 1994; Rees & Mészáros 1994). Nevertheless, the maximal variation of Γ is at the jet boundary and it is where we can expect the most intensive energy release. The jet bulk energy can be dissipated in principle through the acceleration of charged particles (Berezhko 1990; Ostrowski 2000; Stawarz & Ostrowski 2002). If Thomson opacity is sufficiently large, the standard radiation viscosity can also cause the energy dissipation in the boundary layer as, for example, discussed by Arav & Begelman (1992). In the case of AGN jets the Thomson opacity is, however, insufficient to provide the efficient reflection of photons crossing the boundary of the jet. Here we show that the role of the 'mirror' can be played by the soft radiation, which provides the pair production opacity for the high-energy photons.

★E-mail: stern@bes.asc.rssi.ru (BES); juri.poutanen@oulu.fi (JP)

We study the mechanism of shear flow energy dissipation numerically in the same way as it was done by Stern (2003) for shocks. The problem formulation differs in its geometry (tangential jump of the fluid velocity instead of the head-on shock) and in the character of the primary photon background. The complete solution of the problem should account for the feedback of particles on the fluid dynamics and requires detailed numerical treatment of the hydrodynamical part of the problem. In this first study, we neglect internal pressure and consider a one-dimensional dust approximation. With this simplified treatment of hydrodynamics we formulate our problem in the following way. We start from a non-radiating, idealized cylindrical, homogeneous jet and then track its evolution to check whether it produces a runaway photon breeding or not. This numerical experiment is sufficient to demonstrate that under certain circumstances a non-radiating jet cannot exist: it must radiate away a substantial fraction of its kinetic energy.

We present the model of the jet and the environment and formulate the quantitative problem to be solved in Section 2. In Section 3, we describe the proposed mechanism qualitatively, formulate the necessary conditions needed for its operation and provide a simplified analytical study of separate parts of the mechanism. In Section 4, we give the details of the numerical method for simulation of the entire process. The results of numerical simulations for two representative sets of parameters, which show a runaway regime are presented in Section 5. We discuss the results, problems with the model and possible effects in more realistic situations in Section 6, and we conclude in Section 7.

2 MODEL OF THE JET AND THE ENVIRONMENT

We consider a jet of Lorentz factor Γ consisting of cold electrons and protons and the magnetic field. We consider a piece of the jet centred at distance R from the central source and length $20R_\mathrm{j}$, where the jet radius is $R_\mathrm{j} = R\theta$ and θ has the meaning of the opening angle, while for simplicity we approximate the jet by a cylinder of radius R_j. We choose parameters corresponding to the case of AGN taking the distance scale $R \sim 10^{17}$ cm, $\Gamma \sim 10$–20 and $\theta = 0.05$. The radial distance from the jet axis r and the distance from the central source z is measured in units of R_j. The unit of time is R_j/c.

The jet propagates through the soft radiation field, which energy flux we denote $F(x)$, so that $F(x)\,\mathrm{d}x$ is the energy flux in the interval $\mathrm{d}x$. The photon energies, in units of the electron rest mass $m_\mathrm{e}c^2$, are denoted as x and ϵ for photons of low (<1) and high (>1) energies, respectively. We define also the power-law index $\alpha \equiv -\mathrm{d}\log F(x)/\mathrm{d}\log x$.

The radiation field in AGNs has two major components. The first component originates in the accretion disc around the central source and its photons propagate along the jet direction. We consider a standard accretion disc (Shakura & Sunyaev 1973), assuming a simple power law $T(R) \propto R^{-3/4}$ dependence of temperature on radius, with the ratio of the outer to inner disc radius $R_\mathrm{out}/R_\mathrm{in} = 10^4$ and the maximum temperature of $T = 5$eV. The dimensionless temperature is then $\Theta \equiv kT/m_\mathrm{e}c^2 \approx 10^{-5}$. The resulting multicolour disc spectrum $F_\mathrm{d}(x)$ has a power-law shape with energy index $-1/3$ below Θ and has a Rayleigh–Jeans part at energies below $\Theta_\mathrm{min} = \Theta(R_\mathrm{out}/R_\mathrm{in})^{-3/4} \approx 10^{-8}$.

The second, isotropic component consists of the disc radiation scattered and reprocessed in the broad line region (BLR) and the infrared radiation by the dust (Sikora, Begelman & Rees 1994; Sikora et al. 1996). We take its energy density to be a fraction η_i of the energy density of the direct disc radiation, and its flux to be a cut-off power law $F_\mathrm{iso}(x) \propto x^{-\alpha}\exp(-x/x_\mathrm{max})$ extending from the far-infrared $x_\mathrm{min} \sim 10^{-9}$ to the UV band, as we assume $x_\mathrm{max} = \Theta$.

The jet kinetic luminosity scales with the disc luminosity as

$$L_\mathrm{K} = \eta_\mathrm{K} L_\mathrm{d} = \Gamma \dot{M} c^2. \quad (1)$$

From the mass conservation (for a two-sided jet) $\dot{M} = 2\pi\theta^2 R^2 m_\mathrm{p} c n_\mathrm{p}(R)$, we get the Thomson optical depth across the jet from the electrons associated with protons

$$\tau_\mathrm{T}(R) = n_\mathrm{p}(R)\sigma_\mathrm{T} R_\mathrm{j} = \frac{2.4\times10^{-5}\eta_\mathrm{K} L_\mathrm{d,45}}{R_{17}\theta\Gamma}, \quad (2)$$

where we use standard notations $Q = 10^x Q_x$ in cgs units.

Comoving value of the magnetic field in the jet is B_j, its direction is transversal by assumption. A reasonable scaling for the jet field is $B_\mathrm{j} \propto 1/R_\mathrm{j}$, then the Poynting flux carried by the jet

$$L_\mathrm{B} = \eta_\mathrm{B} L_\mathrm{d} = \frac{B_\mathrm{j}^2}{8\pi} 2\pi R_\mathrm{j}^2 \Gamma^2 c \sim 8\times10^{43} B_\mathrm{j}^2 R_{17}^2 (\theta\Gamma)^2 \ \mathrm{erg\ s^{-1}} \quad (3)$$

is constant along the jet. Parameter η_B defines the role of the magnetic field and we consider two cases with low and high η_B.

For our analysis we consider two reference frames: the ambient medium (external) frame and the frame comoving with the fluid with Lorentz factor Γ (jet frame). Energies are normally given in the external frame. The jet comoving values are specified using subscript 'c' or a prime.

3 STEP-BY-STEP DESCRIPTION OF THE BREEDING CYCLE

The solution of the problem of the jet interaction with the external environment and dissipation of its kinetic energy into high-energy radiation requires full-scale non-linear Monte Carlo simulations as described in Section 4. However, it would be useful to perform a simplified analytical study. Very schematically, the process can be split into five steps (see Fig. 1).

(1) A high-energy external photon (which origin is not important) enters the jet and interacts with a soft photon producing an electron–positron pair.

(2) In the jet frame, the produced e^+ and e^- originally move backwards relative to the direction of jet propagation with the energy $\sim\Gamma$ times higher than the energy of the parent photon (in the external frame). When particles gyrate in the magnetic field of the jet, their time-averaged energy, as measured in the external frame, becomes $\sim\Gamma^2$ higher than the parent photon energy.

(3) The pair Comptonizes soft photons up to high energies.

(4) Some of these photons leave the jet and produce pairs in the external environment.

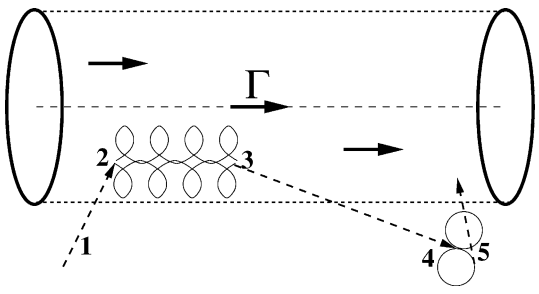

Figure 1. The scheme of the photon breeding cycle. The cylindrical jet moves to the right with a Lorentz factor Γ. The size of the Larmor orbit is highly exaggerated. See Section 3 for details.

(5) Pairs gyrate in the external environment and Comptonize soft photons more or less isotropically. Some of the Comptonized high-energy photons enter the jet again. This step completes the cycle.

Steps 1, 3, 4 and 5 require a field of soft photons to provide the conversion of the high-energy photons into pairs and to produce new high-energy photons through the inverse-Compton scattering. In our case, the direct disc radiation provides the opacity for the high-energy photons at step 1 and provides a target for Compton scattering at step 5. Because the disc radiation is directed along the jet, its effect at steps 3 and 4 is small (interactions are suppressed by the factor of $\sim 1/\Gamma^2$). The isotropic soft photon component provides the major source of seed soft photons for Comptonization at step 3 and the opacity at step 4 as well as contributes to the pair production at step 1.

An additional condition for high efficiency of the cycle is the presence of a transversal or chaotic magnetic field, both in the jet (to provide step 2) and in the external environment (to provide isotropization of pairs and photons Comptonized by them at step 5).

Each step can be characterized by its energy transmission coefficient c_i defined (in the external frame) as the average ratio of total energy of particles with energy above the pair production threshold before and after the step. c_2 is large ($\sim\Gamma^2$), others are smaller than 1. If the criticality index $\overline{C} \equiv c_1 \times c_2 \times c_3 \times c_4 \times c_5 > 1$, then the regime is supercritical, i.e. each cycle produces more particles than the previous one and their number grows exponentially. In this case, we deal with particle breeding rather than with particle acceleration. The spectrum of particles changes slowly (and in principle the mean particle energy can decrease), but the number and the total energy of particles grow rapidly.

Each coefficient c_k can be represented as an average of the energy-dependent coefficient $C_k(\epsilon)$ over the photon spectrum at the kth step

$$c_k = \int C_k(\epsilon) F_k(\epsilon)\, \mathrm{d}\epsilon, \tag{4}$$

where $F_k(\epsilon)$ is the energy flux spectrum at the kth step normalized to unity. The spectrum is a matter of a self-consistent treatment of the whole breeding cycle and we cannot estimate it a priori. For simplicity, we estimate $C_k(\epsilon)$ for the constant external photon field (disc as well as isotropic).

A quantitative example for $C_k(\epsilon)$ behaviour described in this section is given for the same parameters as in the detailed simulation presented in Section 5.1: $L_{\mathrm{d},45} = 1$, $R_{17} = 2$, $\Gamma = 10$, $\theta = 0.05$, $\eta_{\mathrm{K}} = 1$, $\eta_{\mathrm{B}} = 0.01$, $\eta_{\mathrm{i}} = 0.05$, and we consider here two cases of the isotropic photon spectrum with $\alpha = 0.4$ and 1. The value $\alpha = 0.4$ seems reasonable for the BLR region, where the scattered radiation should be dominated by the UV and optical component and some less-energetic IR radiation of dust is expected, while $\alpha = 1$ could be reasonable at the parsec scale where dust radiation can be very important.

3.1 Steps 1 and 4: propagation of photons and pair production

Let us consider a problem of photon propagation through the boundary between the external medium and the jet. Let $a_{\gamma\gamma}(\epsilon)$ be the total opacity for the pair production (i.e. the absorption coefficient produced by the disc and isotropic components) for a photon of energy ϵ. The opacity produced by the isotropic component of the radiation field only is denoted as $a^{\mathrm{iso}}_{\gamma\gamma}(\epsilon)$.

The jet photons move within the cone of opening angle $1/\Gamma$ to the jet direction and interact mostly with the isotropic component of the external radiation field, because the probability of interaction with the disc component is reduced by the factor of $\sim 1/\Gamma^2$. The corresponding opacity computed for the interval perpendicular to the jet direction is $a_{\mathrm{j}} \approx \Gamma a^{\mathrm{iso}}_{\gamma\gamma}(\epsilon_{\mathrm{j}})$. The probability that the jet photon is absorbed in the interval $\mathrm{d}\varpi$ at distance ϖ from the jet boundary is exponential $\exp(-a_{\mathrm{j}}\varpi) a_{\mathrm{j}}\, \mathrm{d}\varpi$ (this assumes that all photons cross the boundary at the same angle $1/\Gamma$). The pair production and consequent Compton scattering transform this photon to photons of energy ϵ_{e}. Roughly half of these photons are emitted towards the jet and the fraction $\exp(-a_{\mathrm{e}}\varpi)$ reaches the boundary [where $a_{\mathrm{e}} = a_{\gamma\gamma}(\epsilon_{\mathrm{e}})$ is the absorption opacity and we assumed that the photons propagate in the direction perpendicular to the boundary]. The probability that the photons are absorbed within the jet is about $1 - \exp(-a_{\mathrm{e}} R_{\mathrm{j}})$. Assuming that only photons born at a distance not more than the jet radius from the boundary can enter the jet, we get the total probability for an external photon of energy ϵ_{e} to interact inside the jet with a soft photon producing an electron–positron pair:

$$\begin{aligned} C_1(\epsilon_{\mathrm{e}}, \epsilon_{\mathrm{j}}) &\approx \int_0^{R_{\mathrm{j}}} \mathrm{e}^{-a_{\mathrm{e}}\varpi} \frac{1}{2} \mathrm{e}^{-a_{\mathrm{j}}\varpi} a_{\mathrm{j}}\, \mathrm{d}\varpi \left(1 - \mathrm{e}^{-a_{\mathrm{e}} R_{\mathrm{j}}}\right) \\ &= \frac{1}{2} \frac{b}{1+b} \left(1 - \mathrm{e}^{-a_{\mathrm{e}} R_{\mathrm{j}}}\right) \left(1 - \mathrm{e}^{-(a_{\mathrm{e}} + a_{\mathrm{j}}) R_{\mathrm{j}}}\right), \end{aligned} \tag{5}$$

where

$$b = \frac{a_{\mathrm{j}}}{a_{\mathrm{e}}} = \frac{\Gamma a^{\mathrm{iso}}_{\gamma\gamma}(\epsilon_{\mathrm{j}})}{a_{\gamma\gamma}(\epsilon_{\mathrm{e}})}. \tag{6}$$

Obviously, C_1 depends also on the energy of the parent photon ϵ_{j}, because it defines the spacial distribution of sources of photons ϵ_{e}.

Analogously, we derive the probability of a high-energy photon ϵ_{j} produced in the jet to escape from the jet and to produce a pair in the external medium at a distance not more than the jet radius from the boundary

$$\begin{aligned} C_4(\epsilon_{\mathrm{j}}, \epsilon_{\mathrm{e}}) &\approx \int_0^{R_{\mathrm{j}}} \mathrm{e}^{-a_{\mathrm{j}}\varpi} \frac{1}{2} \mathrm{e}^{-a_{\mathrm{e}}\varpi} a_{\mathrm{e}}\, \mathrm{d}\varpi \left[1 - \mathrm{e}^{-a_{\mathrm{j}} R_{\mathrm{j}}}\right] \\ &= \frac{1}{2} \frac{1}{1+b} \left[1 - \mathrm{e}^{-a_{\mathrm{j}} R_{\mathrm{j}}}\right] \left[1 - \mathrm{e}^{-(a_{\mathrm{e}} + a_{\mathrm{j}}) R_{\mathrm{j}}}\right]. \end{aligned} \tag{7}$$

Again, C_4 depends on the energy of the parent photon ϵ_{e} that gave rise to the photon ϵ_{j} in the jet.

If opacity is sufficiently high (i.e. we can ignore exponential factors in equations 5 and 7), the sum of the probabilities $C_1(\epsilon_{\mathrm{e}}, \epsilon_{\mathrm{j}}) + C_4(\epsilon_{\mathrm{j}}, \epsilon_{\mathrm{e}}) = 1/2$, and their product reaches the maximum of $1/16$ when the opacities are equal, $b = 1$. Accounting for the angular distribution of photons gives

$$\max[C_1(\epsilon_{\mathrm{e}}, \epsilon_{\mathrm{j}})\, C_4(\epsilon_{\mathrm{j}}, \epsilon_{\mathrm{e}})] \approx \frac{1}{21}. \tag{8}$$

Let us now discuss in details the behaviour of the photon opacity. For isotropic external photons, the main contribution to the photon opacity is given by the radiation of the accretion disc $F_{\mathrm{d}}(x)$. The angle-averaged cross-section of photon–photon pair production $\sigma_{\gamma\gamma}(\epsilon, x)$ has a low-energy threshold $x\epsilon > 1$ and reaches the maximum $\approx 0.21\sigma_{\mathrm{T}}$ at $x\epsilon \approx 3.5$ (see e.g. Zdziarski 1988). The absorption coefficient for a photon of energy ϵ can be obtained by integrating the cross-section over the spectrum of soft photons:

$$a_{\gamma\gamma}(\epsilon) = N_{\mathrm{ph}} \sigma_{\mathrm{T}} \overline{s}_{\gamma\gamma}(\epsilon), \tag{9}$$

where the mean cross-section (in units of σ_{T})

$$\overline{s}_{\gamma\gamma}(\epsilon) = \int_{1/\epsilon}^{\infty} n(x) \sigma_{\gamma\gamma}(x\epsilon)\, \mathrm{d}x \tag{10}$$

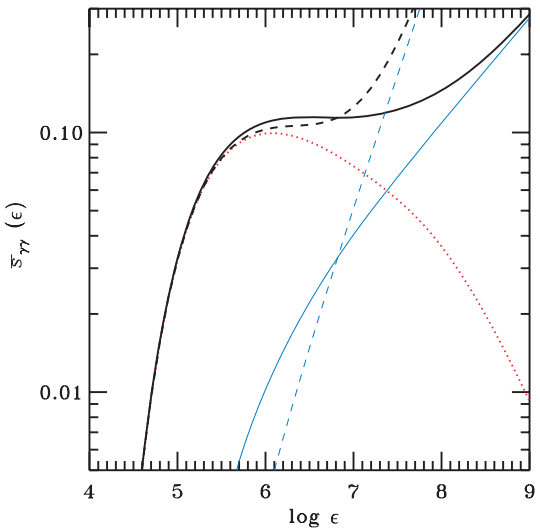

Figure 2. The averaged over the photon distribution photon–photon absorption cross-section $\bar{s}_{\gamma\gamma}(\epsilon)$ given by equation (10). The dotted curve gives the cross-section averaged over the multicolour disc spectrum with $\Theta = 10^{-5}$ and $R_{\rm out}/R_{\rm in} = 10^4$. Almost straight lines give the opacity induced by the isotropic component of the radiation field $\propto \epsilon^{\alpha} \exp(-1/\epsilon\Theta)$ (scaled by the ratio of photon densities $N_{\rm ph,iso}/N_{\rm ph,d}$ of the isotropic and disc radiation). Thick curves give the sum of the two opacities. Solid and dashed lines are for $\alpha = 0.4$ and 1, respectively.

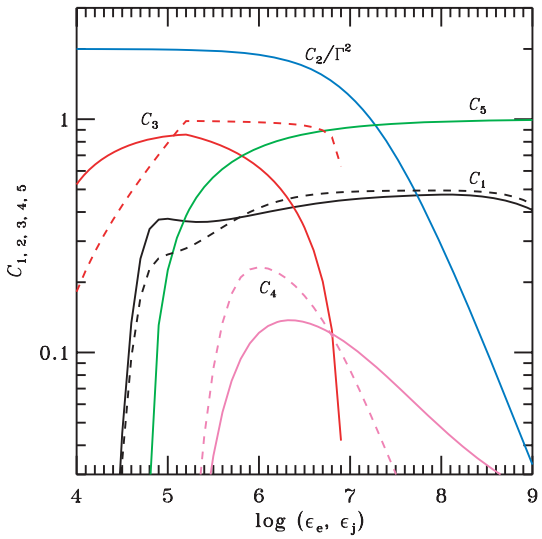

Figure 3. Coefficients $C_i(\epsilon)$ versus photon energy. C_2 and C_3 are functions of energy of a photon produced in the external medium $\epsilon_{\rm e}$, while C_5 is the function of a typically higher photon energy $\epsilon_{\rm j}$, produced in the jet. Coefficients C_1 and C_4 depend on both energies, and we plot here only the one-dimensional cross-sections $C_1(\epsilon_{\rm e}, 10\epsilon_{\rm e})$ and $C_4(\epsilon_{\rm j}, \epsilon_{\rm j}/10)$. Solid curves represents the case $\alpha = 0.4$, while dashed curves are for $\alpha = 1$ (C_2 and C_5 do not depend on the choice of α).

and $n(x)$ is the photon number density normalized to unity. The mean cross-section for the multicolour disc is plotted in Fig. 2 by the dotted curve. The total disc photon number density can be expressed through the energy density $N_{\rm ph,d} = \xi U_{\rm d}/kT$, where $\xi \approx 1.4$ for the multicolour disc. Because $U_{\rm d} = 2L_{\rm d}/(c4\pi R^2)$ close to the jet axis (a factor of 2 comes from the angular distribution of the disc radiation, which we assume to follow the Lambert law), we obtain

$$a_{\gamma\gamma}(\epsilon) = \frac{L_{\rm d}}{c4\pi R^2}\frac{\sigma_{\rm T}}{m_{\rm e}c^2}\frac{1}{\Theta}\,2\,\xi\,\bar{s}_{\gamma\gamma}(\epsilon)$$
$$= 6\times10^{-14}\frac{L_{\rm d,45}}{R_{17}^2\Theta_{-5}}\bar{s}_{\gamma\gamma}(\epsilon)\ {\rm cm}^{-1}. \quad (11)$$

The opacity is low at $\epsilon < 1/\Theta \sim 10^5$ and has a maximum at $\epsilon_{\rm max} \approx 10/\Theta$: $a_{\gamma\gamma,{\rm max}} = 6\ 10^{-15}L_{\rm d,45}/(R_{17}^2\Theta_{-5})\,{\rm cm}^{-1}$. At higher energies $\epsilon > \epsilon_{\rm max}$, the photons interact with the power-law part of the multicolour disc spectrum resulting in a power-law decay of the opacity

$$a_{\gamma\gamma}(\epsilon) \approx a_{\gamma\gamma,{\rm max}}\left(\frac{\epsilon_{\rm max}}{\epsilon}\right)^{1/3}, \quad (12)$$

which transforms into a faster $\frac{1}{\epsilon}\ln\epsilon$ decay at $\epsilon > 1/\Theta_{\rm min}$.

In spite of a lower energy density, the isotropic component $F_{\rm iso}(x)$ dominates the opacity at very high ϵ, because of its much softer spectrum $\alpha > -1/3$. The opacity increases with energy following a power law (Svensson 1987):

$$a_{\gamma\gamma}^{\rm iso}(\epsilon) \approx \frac{1}{5}\frac{\sigma_{\rm T}}{m_{\rm e}c^3}F_{\rm iso}(1/\epsilon) \propto \epsilon^{\alpha}, \quad (13)$$

as shown in Fig. 2.

Because the coefficients C_1 and C_4 depend on both photon energies $\epsilon_{\rm e}$ and $\epsilon_{\rm j}$, it is easier to visualize them as one-dimensional cross-sections. As an example, we plot $C_1(\epsilon_{\rm e}, 10\epsilon_{\rm e})$ and $C_4(\epsilon_{\rm j}, \epsilon_{\rm j}/10)$ in Fig. 3. Coefficient C_1 vanishes below $\epsilon_{\rm e} \ll \epsilon_{\rm max}$, because of low opacity when the photons escape freely and do not produce pairs within the jet. In the interval $5\times10^4 < \epsilon_{\rm e} < 10^6$, $C_1 \sim b/2(1+b) \sim 1/4$ because here the ratio of opacities $b \sim 1$. At higher energies, the opacity is dominated by the isotropic component, $b \approx \Gamma a_{\gamma\gamma}^{\rm iso}(\epsilon_{\rm j})/a_{\gamma\gamma}^{\rm iso}(\epsilon_{\rm e}) \sim \Gamma\ (\epsilon_{\rm j}/\epsilon_{\rm e})^{\alpha}$ is large and $C_1 \sim 1/2$.

Coefficient C_4 vanishes at $\epsilon_{\rm j} < 2\times10^5$ because the opacity produced by the isotropic power-law component is low here, and photons are escaping too far from the jet (note the exponential factor in equation 7). At $\epsilon_{\rm j} \sim 10^6$, $b \sim 1$ and $C_4 \sim 1/4$. At high energies C_4 decays $\propto 1/2b$. In our formulation of C_4, we accounted only for photons that can directly penetrate from the jet to the external medium. However, those high-energy photons that are absorbed within the jet do not leave the system, but produce pair-photon cascade. During the cascade, the photon energy eventually becomes sufficiently low to allow the photon escapes from the jet and produces a pair outside. Thus even if a photon was emitted towards the jet axis, a fraction of its energy can eventually escape the jet in a form of secondary photons.

3.2 Step 2: energy gain of a pair produced in the jet

A high-energy photon of energy $\epsilon_{\rm e}$ at this stage has interacted with a soft photon inside the jet to produce an electron–positron pair. The two particles move now backwards relative to the jet propagation direction with the mean comoving Lorentz factor

$$\gamma_{\rm c} = \frac{4}{3}\frac{\epsilon_{\rm e}}{2}\Gamma. \quad (14)$$

Here the factor of 4/3 comes from the averaging over the angles of the incident high-energy photons accounting for the probability of interaction with the disc photons moving along the jet (in case of interaction with the isotropic photon field, this factor disappears). Integrating over the Larmor orbit, we get the mean particle energy in the external frame

$$\langle\gamma\rangle = \gamma_{\rm c}\Gamma\left\langle(1+\cos\phi_{\rm c})^2\right\rangle_{\phi_{\rm c}} = \frac{3}{2}\gamma_{\rm c}\Gamma = 2\frac{\epsilon_{\rm e}}{2}\Gamma^2, \quad (15)$$

where ϕ_c is the angle between the particle momentum and jet propagation direction (in jet frame). Note, that the averaging is over ϕ_c, not $\cos\phi_c$. The mean energy gain is then

$$C_2(\epsilon_e) = \frac{\langle\gamma\rangle}{\epsilon_e/2} = 2\Gamma^2. \quad (16)$$

The time-scale of synchrotron cooling is equal to the inverse of Larmor frequency at the (comoving) electron Lorentz factor

$$\gamma_{c,max} \approx 10^8 B_j^{-1/2}. \quad (17)$$

Compton losses because of the disc radiation can be neglected at this step (for our parameters) due to a deep Klein–Nishina regime of scattering at $\gamma_c \gtrsim 10^8$. For a very high initial photon energy $\epsilon_e \gg \gamma_{c,max}\Gamma$, the Lorentz factor of the produced pair is reduced to $\sim\gamma_{c,max}$ after first Larmor orbit because of the synchrotron losses. In the external frame its energy is now $\sim\gamma_{c,max}\Gamma$, resulting in the energy gain (loss) factor $C_2(\epsilon_e) \approx \gamma_{c,max}\Gamma/\epsilon_e$. Thus, the energy gain for arbitrary ϵ_e (shown in Fig. 3) can be written as

$$C_2(\epsilon_e) = 2\Gamma^2 \frac{1}{1+\epsilon_e\Gamma/\gamma_{c,max}}. \quad (18)$$

3.3 Step 3: energy conversion into photons

Coefficient $C_3(\epsilon_e)$ describes a fraction of the electron (positron) energy, which is converted into photons with the energy above the thresholds of the cycle $\epsilon_{j,min} = 3 \times 10^5$ defined by a sharp drop of coefficient C_4. Photons of lower energies escape almost freely from the jet and are lost from the cycle. C_4 also drops above $\sim 3 \times 10^7$, however, the photons of higher energies are not lost from the cycle, but produce a pair cascade and eventually escape from the jet producing pairs outside.

The efficiency of conversion is mainly determined by the ratio between Compton and synchrotron losses (because synchrotron photon energy is below $\epsilon_{j,min}$ in our case), which, in Thomson regime, is just the ratio of the soft radiation energy density (dominated by the isotropic component) to the magnetic field energy density (measured in the jet frame):

$$\frac{U'_{rad}}{U'_B} = \frac{\eta_i U_d \Gamma^2}{L_B/\left(2\pi R_j^2 \Gamma^2 c\right)} = \frac{\eta_i}{\eta_B}(\Gamma\theta)^2\Gamma^2. \quad (19)$$

In reality, however, the share of Compton scattering is much smaller, because a pair produced in the jet by a photon at $\epsilon_e \sim 1/\Theta$ gains energy up to $\gamma \sim \Gamma^2/\Theta$ and interacts with photons at $x \sim \Theta$ in the deep Klein–Nishina regime. The situation also complicates by the fact, that because of cooling, the fraction of soft photons interacting with the pair in Thomson regime grows with time.

Neglecting for simplicity scattering in the Klein–Nishina regime and pair cooling (i.e. assuming a constant pair Lorentz factor given by equation 14), we define the coefficient C_3 as the ratio of the soft radiation energy density, that can produce photons above the threshold, to the sum of the magnetic field energy density and the total radiation density in the Thomson regime

$$C_3(\epsilon_e) = \frac{U'_{cycle}}{U'_B + U'_T}, \quad (20)$$

where

$$U'_B = \frac{B_j^2}{8\pi}, \quad (21)$$

$$U'_T \propto \Gamma^2 \int_{x_{min}}^{x_{KN}} F_{iso}(x)\,dx, \quad (22)$$

$$U'_{cycle} \propto \Gamma^2 \int_{\max[x_{min},x_{low}]}^{x_{KN}} F_{iso}(x)\,dx. \quad (23)$$

The upper integration limits is defined by the Thomson regime of scattering

$$x < x_{KN} = \frac{1}{\langle\gamma\rangle} = \frac{1}{\epsilon_e\Gamma^2}. \quad (24)$$

The lower limit is given by the condition that the scattered photon energy $\epsilon_j = x\,\langle\gamma^2\rangle$ is above the threshold $\epsilon_{j,min}$. Averaging over the Larmor orbit, we get the mean square of the particle Lorentz factor

$$\langle\gamma^2\rangle = \gamma_c^2\Gamma^2\,\langle(1+\cos\phi_c)^3\rangle_{\phi_c} = \frac{5}{2}\gamma_c^2\Gamma^2 = \frac{10}{9}\epsilon_e^2\Gamma^4, \quad (25)$$

that gives

$$x > x_{low} = \frac{\epsilon_{j,min}}{\langle\gamma^2\rangle} = \frac{9}{10}\frac{\epsilon_{j,min}}{\epsilon_e^2\Gamma^4}. \quad (26)$$

The behaviour of $C_3(\epsilon_e)$ is shown in Fig. 3.

There are three characteristic energies. For $\epsilon_e < \epsilon_1 \approx \epsilon_{j,min}/\Gamma^2 \sim 10^3$, $x_{KN} < x_{low}$ and C_3 vanishes. At energies $\epsilon_e > \epsilon_2 \approx \sqrt{\epsilon_{j,min}/x_{min}}/\,\Gamma^2 \sim 10^5$, $U_T = U_{cycle}$ because $x_{low} < x_{min}$. And at energies above $\epsilon_3 = 1/(\Gamma^2 x_{min}) \sim 10^7$, $x_{KN} < x_{min}$ and $C_3 = 0$ in our approximation. At energies $\epsilon_2 < \epsilon_e < \epsilon_3$, one can approximate

$$\frac{1}{C_3(\epsilon_e)} \approx \begin{cases} 1 + \dfrac{U'_B}{U'_{rad}}\dfrac{x_{max}^{1-\alpha} - x_{min}^{1-\alpha}}{x_{KN}^{1-\alpha} - x_{min}^{1-\alpha}}, & \alpha \neq 1, \\ 1 + \dfrac{U'_B}{U'_{rad}}\dfrac{\ln(x_{max}/x_{min})}{\ln(x_{KN}/x_{min})}, & \alpha = 1. \end{cases} \quad (27)$$

Taking into account equation (19), we can conclude that the Comptonization at step 3 can be very efficient ($C_3 \sim 1$) if the following conditions are satisfied.

(i) The magnetic field is weak, $\eta_B \ll 1$.

(ii) The energy density of the external isotropic radiation is large in the jet frame, i.e. Γ or η_i are large.

(iii) The spectrum of isotropic component is soft, $\alpha \gtrsim 1$. Then the power-law decay of C_3 above ϵ_2 is replaced by a constant or a logarithmic decay (see equation 27 and note a slow decays of C_3 in Fig. 3, dashed curve). In this case, a high value of C_3 is possible even for the magnetically dominated jet if its total power is a few times smaller than the disc luminosity.

3.4 Step 5: Compton scattering in the external environment

At step (5) an electron–positron pair, produced in the external enviroment, Comptonizes a number of soft photons to produce high-energy photons above the energy threshold $\epsilon_{e,min} \sim 3\,10^4$ defined by the low-energy cut-off of C_1. At this step, synchrotron losses which can be safely neglected as magnetic field in the external medium is much lower than the jet field.

Because the cooling is fast, the spectrum produced by a pair is a standard 'cooling' spectrum $F(\epsilon) \propto \epsilon^{-1/2}$ extending up to the maximum energy equal to the pair Lorentz factor $\gamma = \epsilon_j/2$. Defining coefficient $C_5(\epsilon_j)$ as the energy fraction emitted above the thresholds $\epsilon_{e,min}$, we get

$$C_5(\epsilon_j) = 1 - \left(\frac{\epsilon_{e,min}}{\gamma}\right)^{1/2} = 1 - \left(\frac{2\epsilon_{e,min}}{\epsilon_j}\right)^{1/2}. \quad (28)$$

The computed $C_5(\epsilon_j)$ is shown in Fig. 3. A low-energy cut-off is at $\epsilon_j = 2\,\epsilon_{e,min} = 6 \times 10^4$.

3.5 Amplification through the cycle and dissipation efficiency

The absolute theoretical maximum of the amplification factor

$$\max A(\epsilon_e, \epsilon_j) = C_1C_2C_3C_4C_5 \approx \frac{\Gamma^2}{10} \quad (29)$$

is achieved when $C_2 = 2\,\Gamma^2, C_1 \times C_4 = 1/21$ and $C_3 = C_5 = 1$. Thus, the minimum jet Lorentz factor required to achieve supercriticality is $\Gamma \approx 3$. In a more realistic situation, the amplification factor is smaller and larger Γ is needed. For example, a strong magnetic field inhibits the photon breeding reducing C_2 and C_3 because of synchrotron losses. The cascade still develops, if a sufficiently dense soft external radiation field is present, because $C_3 \sim 1$, when $\eta_i\Gamma^4/\eta_B$ is large (Section 3.3), see Section 5.2 for the simulation example.

An estimation of A using our simple formulae from Sections 3.1–3.4 is shown in Fig. 4. For $\alpha = 0.4$, it reaches 7.4 at $\epsilon_e = 2\ 10^5$, $\epsilon_j = 10^6$ (the more precise Monte Carlo step-by-step simulations of the cycle efficiency show A reaching the maximum of 4.7 at $\epsilon_e = 5\,10^5, \epsilon_j = 2\,10^6$). For $\alpha = 1$, the maximum of A is about 9.9 at $\epsilon_e = 3\ 10^5, \epsilon_j = 2\ 10^6$. Of course, $A(\epsilon_e, \epsilon_j)$ does not have the meaning of the criticality index $\overline{C}$. The photon energy distribution during the cycle is wide and does not necessarily coincide with the area of the maximal amplification. Fig. 4 (dotted curve) shows the median energy $\epsilon_j(\epsilon_e)$ computed by a Monte Carlo method (for $\alpha = 0.4$) of the distribution $\epsilon_j p_{23}(\epsilon_j, \epsilon_e)$, where $p_{23}(\epsilon_j, \epsilon_e)$ is the probability density of a photon of energy ϵ_e to produce a photon of energy ϵ_j after steps 2 and 3. A similar function $\epsilon_e(\epsilon_j)$ for step 5, which is a median of distribution $\epsilon_e p_5(\epsilon_e, \epsilon_j)$, is also shown (dashed curve). Note that the median energy gain at steps 2 and 3 is slightly higher than the energy loss at step 5, which means that the photon energy rises on average during the cycle and tends to the area at $\epsilon_e \sim 3\,10^6$, $\epsilon_j \sim 3\,10^7$, where the curves intersect. The amplification in that area is $A(\epsilon_e, \epsilon_j) \approx 2$.

We can now estimate a typical distance where the most efficient energy dissipation in the shear flow should take place. The total optical depth across the jet is (see equation 11)

$$\tau_{\gamma\gamma}(\epsilon) = a_{\gamma\gamma}(\epsilon)R_j = 300\frac{L_{d,45}(20\theta)}{R_{17}\Theta_{-5}}\overline{s}_{\gamma\gamma}(\epsilon), \quad (30)$$

which gives us the maximal distance from the central engine where $\tau_{\gamma\gamma}(\epsilon_{max}) \sim 1$ and, therefore, is sufficient to produce pairs in the jet

$$R_{max} \sim \frac{L_{d,45}\ (20\theta)}{\Theta_{-5}}\ \text{pc}. \quad (31)$$

Note that infrared emission of the dust can provide the opacity for higher energy photons at much larger distances.

At $R < R_{max}$, the typical depth of photon penetration $\delta\varpi = \delta r R_j$ into the jet is given by the condition $\delta\varpi a_{\gamma\gamma}(\epsilon) = 1$, i.e. $\delta r = 1/\tau_{\gamma\gamma}(\epsilon)$. At the peak of absorption, for $\epsilon \sim \epsilon_{max}$, we obtain

$$\delta r = \frac{R}{R_{max}} = 0.03\frac{\Theta_{-5}R_{17}}{L_{d,45}\ (20\theta)}. \quad (32)$$

The value of $2\delta r$ defines the fraction of the jet volume occupied by the 'active layer', which is responsible for the exponential breeding of the high-energy photons. Because the photons of slightly higher and lower energies than ϵ_{max} can propagate further into the jet, the fraction of the total jet kinetic energy released is even higher than $2\delta r$, as demonstrated by the full-scale simulation (see Section 5). At small distances from the central source, opacity is so large that the high-energy photons can hardly penetrate the boundary between the jet and the external medium. The cascade can develop there, but the dissipation efficiency is very low because δr is small.

The efficiency also depends on the number of generations N the breeding cycle operates. A high efficiency is achieved if N is larger than a few (say $N = 10$). The time-scale of the cycle is defined by the longest step 4, which takes on average $t_{cycle} \sim \delta r\,\Gamma$. Because the active layer width depends on distance $\delta r \propto R$, the breeding cycle takes longer time (in R_j/c units) at larger R and at the same time it is less sensitive to the requirement of a sharp boundary. The cycle time-scale should be compared to the dynamical time-scale $t_{dyn} \sim 1/\theta$. This determines the most favourable distance for the breeding to operate as

$$R_{eff} = \frac{R_{max}}{N\Gamma\theta} = \frac{1}{N}\frac{L_{d,45}}{\Theta_{-5}}\frac{20}{\Gamma}\ \text{pc}. \quad (33)$$

For this estimation, we assumed that the amplification factor A does not depend on distance R. This is true as long as B_j^2, F_d and F_{iso} all scale as $1/R^2$ and $\delta r \ll 1$. The last condition breaks down at a parsec scale (see equation 31), while the scaling for F_{iso} probably breaks much closer, as one can hardly expect the existence of the sufficient material to provide efficient scattering/reprocessing of the disc radiation to the isotropic component beyond the BLR. Thus, the most efficient dissipation is expected within the BLR at $R_{eff} < R < R_{max}$.

There still remains such source of F_{iso} as the dust IR radiation, but it cannot convert photons at $\epsilon_j < 10^7$ into pairs and the coefficient C_4 will be small. In such a case one can expect that the cycle works in the TeV range, which could be relevant for TeV blazars. At small distances $R < 10^{16}$ cm, there appears another possibility: non-thermal X-ray component of the disc radiation (which typically constitutes ~0.1 of the disc luminosity) becomes opaque and can efficiently convert lower energy photons ($\epsilon < 1/\Theta$). Then, one can expect the existence of a low-energy breeding cycle in the range $\epsilon \sim 10^3$–10^4. This possibility requires a separate study.

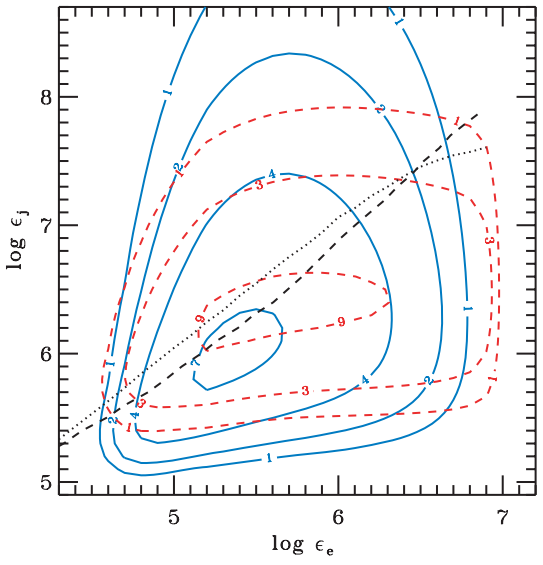

Figure 4. The product of the five coefficients $A(\epsilon_e, \epsilon_j) = C_1(\epsilon_e, \epsilon_j)\,C_2(\epsilon_e)\,C_3(\epsilon_e)\,C_4(\epsilon_j, \epsilon_e)\,C_5(\epsilon_j)$, represented by contours of constant levels. For $\alpha = 0.4$ (solid contours), it reaches the maximum of 7.4 at $\epsilon_e = 2 \times 10^5, \epsilon_j = 10^6$. In this case, the dotted curve shows the median energy $\epsilon_j(\epsilon_e)$ for steps 2 and 3, and the dashed curve shows the median energy $\epsilon_e(\epsilon_j)$ at step 5. For $\alpha = 1$ (dashed contours), the maximum of 9.9 is at $\epsilon_e = 3 \times 10^5, \epsilon_j = 2 \times 10^6$.

4 NUMERICAL IMPLEMENTATION

We assume a sharp boundary between the jet and the surrounding medium at the start of simulations. For simplicity we adopt the

constant physical conditions along the $20R_j$ interval, including a uniform field of the external radiation. The jet decelerates transferring its momentum to the radiation. In our model, we take into account the dependence of the fluid Lorentz factor on r only.

The numerical simulation method is based on the Large Particle Monte Carlo code (LPMC) developed by Stern (1985) and Stern et al. (1995). The code can treat essentially non-linear problems when the simulated particles constitute at the same time a target medium for other particles. The number of large particles (LPs) representing photons and $e^{\pm}$ pairs was $2^{17} = 131\,072$.

The version of LPMC used here treats Compton scattering, synchrotron radiation, photon–photon pair production and pair annihilation. Synchrotron self-absorption was neglected as it consumes too much computing power and is not very important in this application. All these processes are reproduced without any simplifications at the microphysics level. The general organization of the LPMC simulation is described in Stern (1995). A new specific feature of numerical simulation in this work (as well as in Stern 2003) is a scheme of particle tracking in the relativistic fluid.

Parameters of photon LPs are defined in the external reference frame. The energy and the direction of electron/positron LPs are defined in the jet frame, since the electron energy in the external frame oscillates by a factor of $4\Gamma^2$ because of gyration in the magnetic field.

The tracking scheme for the high-energy charged particle LPs differs for the first Larmor orbit and the rest of the trajectory. The reason is that at the first orbit a particle can lose the main fraction of its (jet frame) energy before it turns around and gains the energy in the external frame (see Section 3.2 and equation 17).

Rapid energy losses require a fine particle tracking at the first Larmor orbit if the particle has been produced with $\gamma_c > \gamma_{c,max}$. Therefore, the comoving tracking step is limited by $ds = 0.1R_L$, where $R_L = 1.7\,10^3\gamma_c/B_j$ cm is the Larmor radius. Each step is described in both reference frames. The corresponding Lorentz transformations from the jet frame to the external frame are

$$dt = dt_c\left(1 + \frac{V}{c}\beta_c\cos\phi_c\right)\Gamma, \quad \gamma = \gamma_c\left(1 + \frac{V}{c}\beta_c\cos\phi_c\right)\Gamma, \tag{34}$$

where V is the velocity of the fluid, dt_c is the comoving time interval for the tracking step, β_c is the particle comoving velocity in units of c, ϕ_c is the angle between comoving direction of the particle momentum and the jet, dt and γ are the external frame values for the step time-interval and the particle Lorentz factor. The comoving representation is used to track the particle gyration in the magnetic field frozen into the jet and to simulate the synchrotron radiation. The external frame representation is more convenient to simulate interactions with photons and is necessary to synchronize the particle tracking with the general evolution of the system.

An example of a high-energy ($\gamma_c > \gamma_{c,max}$) particle tracking for several Larmor orbits as viewed from both reference frames is shown in Fig. 5. The magnetic field and the external soft photon field correspond to the case considered in Section 5.1. One can see the dramatic energy loss due to synchrotron radiation at the first orbit and a much slower further evolution. A discrete step at $t \sim 4 \times 10^{-3}$ is a result of Compton scattering.

When the particle energy is below $\gamma_{c,max}$, we can neglect the dependence between the comoving direction and the energy. In this case, we sample the direction of the particle assuming a uniform distribution of its gyration phase ϕ_c in the comoving system. The

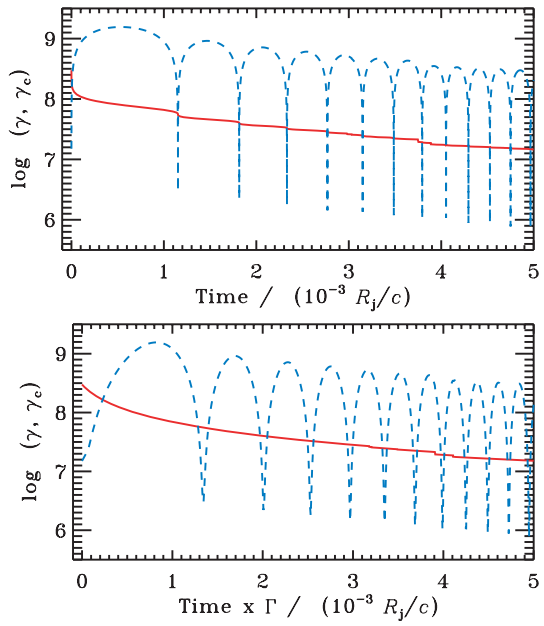

Figure 5. External frame (γ, dashed curve) and jet comoving (γ_c, solid line) Lorentz factor of a particle gyrating in the transversal magnetic field $B_j = 0.35$ G frozen into fluid. Upper panel: dependence on the external frame time. Lower panel: dependence on the comoving time multiplied by the bulk Lorentz factor $\Gamma = 10$. Initial Lorentz factor of the particle is $\gamma_c = 3 \times 10^8$ and the jet radius $R_j = 10^{16}$ cm.

external frame probability density function for ϕ_c is

$$p(\phi_c) \propto \frac{dt}{dt_c} = \left(1 + \frac{V}{c}\beta_c\cos\phi_c\right)\Gamma. \tag{35}$$

Trajectories and momenta of LPs are three-dimensional. The target LP density is averaged over 45 two-dimensional cylindric cells: five layers along the jet with nine concentric shells in each. The trajectories of electrons and positrons in the magnetic field were simulated directly assuming transversal geometry of the field B_j in the jet and B_e in the external matter.

The primary soft photon field (disc and external isotropic) is kept constant during the simulations. Any additional soft (synchrotron) photons produced by the cascade participate in the simulations in the form of LPs. At the start of simulations, the shell of the length $\Delta z = 20$ between $10 < z < 30$, and the radial extend $0.9 < r < 1$ is filled by seed isotropic high-energy photons, whose energy density is several orders of magnitude less than the energy density of the jet. All particles participating in the simulations are descenders of these seed photons. In the course of the simulations, the jet undergoes differential deceleration. We split the jet into 500 cylindric shells, calculate the momentum transferred to each shell and decelerate each shell independently from others.

5 RESULTS OF SIMULATIONS

We have made several tens of simulation runs with different parameters and various model formulations. In some of them we observed the exponential energy grow, others gave no effect. As we have shown in Section 3, the supercritical behaviour appears, when the jet Lorentz factor and the density of the soft isotropic radiation are sufficiently high. The lowest Lorentz factor, where the cascade is

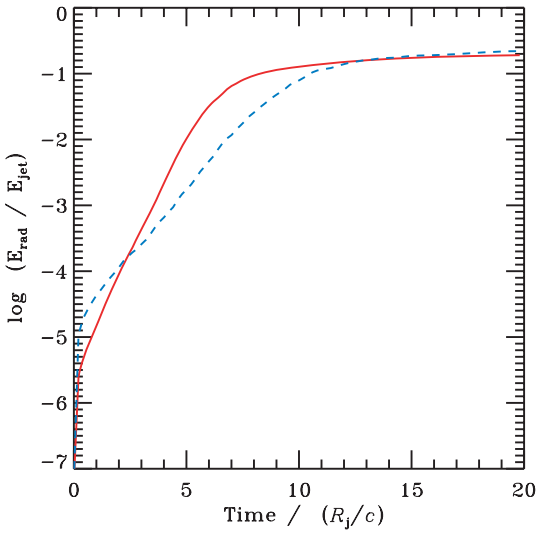

Figure 6. Total cumulative energy release of the fluid into radiation versus time. Solid curve: Example 1 and dashed curve: Example 2 (see text).

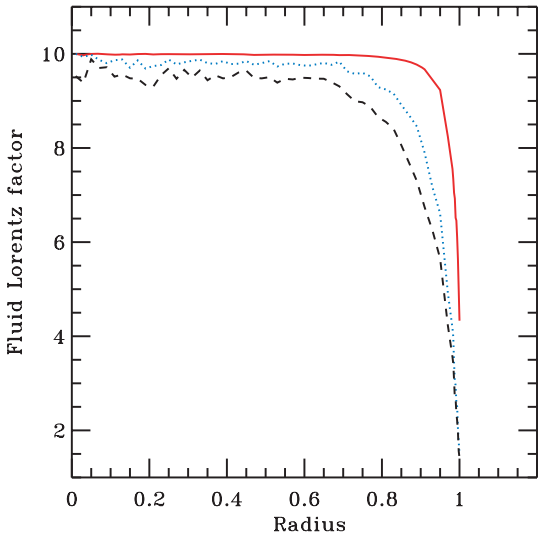

Figure 7. Fluid Lorentz factor versus cylindrical radius of the jet r for Example 1 at various times $t = 6$ (upper curve), $t = 10$ (middle curve) and $t = 20$ (lower curve).

possible in principle is around $\Gamma = 4$. Here, we present only two examples demonstrating the development of the runaway cascade for different conditions.

5.1 Example 1. Weak magnetic field and a 'minimal' seed radiation

In this example, we assume the disc luminosity $L_{\rm d,45} = 1$, the distance of the active region from the black hole $R_{17} = 2$ and jet parameters $\Gamma = 10$, $\theta = 0.05$. The total jet kinetic power is equal to the disc luminosity $\eta_{\rm K} = 1$ and the Poynting flux is one per cent of that $\eta_{\rm B} = 0.01$. This implies a matter-dominated jet. The resulting magnetic field in the jet (comoving frame) is $B_{\rm j} \approx 0.35$ G and we take the external magnetic field $B_{\rm e} = 10^{-3}$ G. The ratio of isotropic and disc radiation energy densities is $\eta_{\rm i} = 0.05$, and we assume $\alpha = 0.4$.

The total (cumulative) energy release as a function of time is shown in Fig. 6. We observe a reasonably fast breeding with e-folding time $t_{\rm e} \sim 0.6$. The active layer is rather thin: a half of the energy release is concentrated within $\delta r \sim 0.02$ from the jet boundary. At $t \sim 6$ the regime changes: the external shell decelerates (see Fig. 7) and the active layer gets wider ($\delta r = 0.05$ at $t = 8$ and $\delta r = 0.08$ at $t = 20$). The cascade breeding slows down as the photon path length through the cycle increases. The total energy release into photons reaches 19 per cent of the total jet energy at the end of simulation at $t = 20$. Simulation demonstrated a significant pair loading at the late stage: the Thomson optical depth of produced pairs across the jet has reached $\sim 3 \times 10^{-5}$ which exceeds the initial depth of electrons associated with protons by 25 per cent (assuming proton-dominated jet, see equation 2). Most of these pairs are loaded in the outer region of the jet ($r > 0.8$), where they dominate the number density of original electrons by a factor of 8.

While the jet decelerates in our model, the external environment is fixed at rest. In reality, it undergoes a radiative acceleration. Fig. 8 shows the momentum exchange between matter and photons. The momentum transferred to the external environment is an order of magnitude less than the momentum losses of the jet to radiation. The momentum gained by the external shell $\delta r = 2 \times 10^{-3}$ around the jet boundary is $\Delta P \approx 10^{48}$ erg/c. The volume of the innermost external

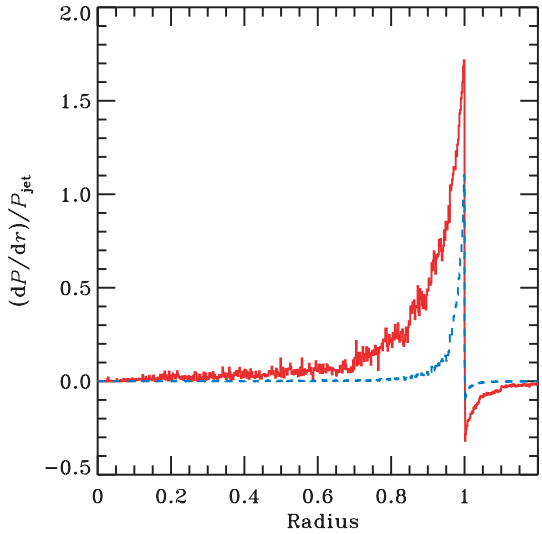

Figure 8. Momentum exchange between the fluid and photons for Example 1. A narrow distribution (dashes) corresponds to time $t = 6$, and a wider distribution is for $t = 20$.

shell is $2\pi R_{\rm j}\ \delta r\ \Delta z \approx 10^{47}$ cm^3. Therefore, the volume density of the transferred momentum is $\sim$10 erg cm$^{-3}/c$. If the density of external medium exceeds 10^4 cm^{-3} (i.e. the energy density $nm_{\rm p}c^2$ is higher than 10 erg cm^{-3}), we can neglect the effects of its acceleration by the deposited momentum.

The evolution of the photon instant spectrum (i.e. the spectrum of photons which are in the volume at the moment) is shown in Fig. 9(a). Early spectrum demonstrates two distinct components: the TeV Comptonization peak (mainly the Compton-scattered external isotropic photons) and the synchrotron maximum. After $t \sim 6$ the spectrum changes: the main peak moves to lower energies and the synchrotron peak declines. The reason for such evolution is evident: the system enters a non-linear stage, because the synchrotron radiation of the cascade exceeds the initial soft photon field. The

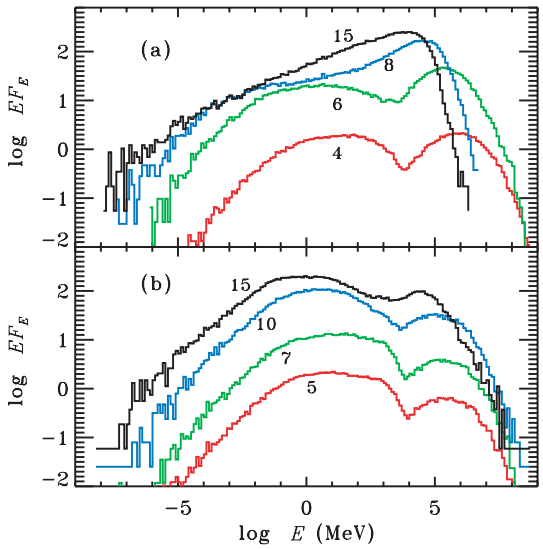

Figure 9. Evolution of the instantaneous (jet frame) photon spectra within the emitting medium. (a) Example 1 and (b) Example 2. The observed spectra should be close to the latest ones. Time in units R_j/c is marked next to the corresponding curves.

Comptonization losses increase, whereas the synchrotron losses do not change.

Note, that an observer cannot see the high-energy part of early spectra because the isotropic radiation field F_{iso} is opaque for photons with energy $\epsilon > 1/\Theta$. The observed spectrum should have such a cut-off in the late spectra. A detection of a sharp cut-off at tens of GeV would be the evidence for gamma-rays origin in quasars (blazars) at the scale of the broad emission-line region.

5.2 Example 2. Strong magnetic field

We consider the same parameters as in Example 1, but take $\eta_B = 1$ implying magnetically dominated jet with Poynting flux $L_B = 10^{45}$ erg s^{-1} (for a two-sided jet). The comoving value of magnetic field is 3.5 G. The ratio of Compton to synchrotron losses at such parameters is low (see Section 3.3). Therefore, the system remains subcritical and the simulations have shown no supercritical photon breeding at such conditions. Our analytical calculations show that the maximum of A is about 0.5. The situation changes if we take a softer spectrum of the isotropic component with $\alpha = 1$, then max $A = 3.5$. If we instead increase the soft photon density to $\eta_i = 0.2$, then max $A = 1.2$. However, the easiest way to achieve criticality is to increase the jet Lorentz factor to $\Gamma = 20$, which gives max $A = 8.4$. All these options increase the importance of the Compton cooling relative to the synchrotron (see equations 19 and 27).

In the numerical simulations, we followed the last alternative. In this case, the comoving magnetic field is 1.75 G. The simulations have shown that the active layer is wider than that in Example 1: $\delta r \sim 0.05$ at the beginning of the evolution (therefore this case is more stable against the mixing of the boundary layer). The exponential growth is slower (see Fig. 6), but the final energy release is the same as in the previous case. The pair loading is an order of magnitude smaller than that in Example 1.

The hard-to-soft evolution of the high-energy peak of the photon spectrum shown in Fig. 9(b) spans almost all the range of peak energies observed in blazars. The latest spectrum peaks in the MeV range as in MeV blazars.

6 DISCUSSION

We have demonstrated that a supercritical runaway cascade develops under reasonable conditions and can convert at least ∼20 per cent of the jet kinetic energy into radiation. This is certainly not an ultimate value: with our simplified model we are able to reproduce only the initial stage of the evolution. Indeed, our cylindric shells decelerate as a whole with constant Lorentz factor along z-axis. Therefore, once the outer shells decelerate, the cascade breeding slows down everywhere. Actually, the radial gradient of Γ should depend on z and a slow breeding at larger z can co-exist with a fast breeding at a smaller z.

The behaviour of the jet is strongly non-linear because the process is very sensitive to a number of details including the geometry of the magnetic field, density of the external environment, density of the isotropic soft photon field, etc. The effect of inhomogeneities, which are exponentially amplified, can be dramatic, particularly taking a form of flares and moving bright blobs and resulting in the formation of internal shocks. A more realistic model should include a detailed treatment of fluid hydrodynamics (at least in 2D) coupled with the electromagnetic cascade.

The model can reproduce the high-energy component of blazar radiation. On the other hand, examples presented in this work do not reproduce the low-energy synchrotron components as prominent as observed in blazars. It is possible that the synchrotron bump is produced at much larger distances from the central source than the Compton component.

A certain problem can appear if the jet boundary is turbulent (see e.g. Aloy et al. 1999): the thin active zone at the jet boundary layer as in above examples does not exist in this case. Then, one still can expect to obtain the supercriticality at a moderate transversal opacity. However, the breeding cycle in this case would take longer than R_j/c. If the electromagnetic cascade grows only along the jet, the active range of z could be insufficient to provide the growth by orders of magnitude. An issue to be studied is whether the cascade can grow *with time* at a fixed z or not. This could be due to a spatial feedback at step 5: a photon from the external environment moves upstream to a smaller z than the point where a parent photon has been produced at step 3. It is clear that such feedback is weak, but in the case of a jet the time is unlimited. Note that even if the supercriticality is not reached, the process can amplify the high-energy output of the charged particle acceleration in the subcritical regime.

Now let us try to characterize in general terms the mechanism we are dealing with. First of all, it belongs to a class of supercritical runaway phenomena like neutron breeding in a nuclear pile or a nuclear explosion. Such phenomena still seem rather exotic in astrophysics (let alone 'trivial' nuclear explosions of supernovae or of the accreting matter at the surface of neutron stars). To our knowledge, there exist only a few works considering such kind of phenomena. Stern & Svensson (1991) discovered with numerical simulations a supercritical behaviour of electromagnetic cascade in a cloud of ultrarelativistic protons with sufficient compactness. In that case, the energy is stored in non-radiating protons and the supercriticality appears in the energy transfer from protons to pairs and photons through photomeson production. Later, this mechanism was confirmed analytically by Kirk & Mastichiadis (1992). However, at that time, there was no clear astrophysical situation providing proper conditions. Recently Kazanas, Georganopoulos & Mastichiadis (2002) have found that a possible site for such a phenomenon could be a highly relativistic shock in gamma-ray bursts.

In this work (see also Stern 2003), we propose a different kind of a supercritical process where the energy is extracted by particles

directly from the kinetic energy of the fluid. In principle, the protons can also participate in such mechanism, especially, if a scheme of Derishev et al. (2003) with $p + \gamma \rightarrow n + \pi^+$ charge exchange works at given conditions. In this case we would have a unified mechanism, where the electromagnetic cascade is fed by the fluid bulk motion directly and through the high-energy nucleons.

In any case, the supercritical models of energy conversion look promising for explanation of such violent phenomena as blazars and gamma-ray bursts because the supercriticality does produce violent effects.

7 CONCLUSIONS

We have proposed and studied a novel photon breeding mechanism of the high-energy emission from relativistic jets. We showed that a relativistic jet moving through the sufficiently dense soft radiation field inevitably undergoes transformation into a luminous state. We have considered the application of this mechanism for the AGN jets, while actually it may also work in microquasars and gamma-ray bursts, if the latter are associated with the well-formed narrow jets. In general, the mechanism can be characterized as a viscous dissipation of the kinetic energy of the jet into high-energy photons. We showed that at least 20 per cent of the jet energy can be converted into high-energy radiation. From the dynamical point of view the mechanism is a supercritical process, which is very similar to the chain reaction in the supercritical nuclear pile. The subject to exponential breeding in our case is electromagnetic cascade, particularly the high-energy photons which create a viscosity between the jet and the external environment.

In the case, when the exponential photon breeding does not occur, the process still could act as a subcritical amplifier for the high-energy output of internal shocks or other mechanisms of particle acceleration. Alternatively, it can produce a population of hot electrons/positrons which can then participate in the Fermi I type of acceleration of charged particles.

The photon breeding mechanism works very efficiently at the following conditions.

(i) The jet Lorentz factor exceeding 3–4.

(ii) A weak magnetic field and/or a large density of the external soft isotropic radiation field.

(iii) If the magnetic field is strong (equipartition or magnetically dominated jet), the supercritical regime requires a dense soft radiation component (in the jet frame), which requires either a large fraction of scattered photons or a large jet Lorentz factor. Alternatively, an additional source of soft photons, e.g. the synchrotron radiation from other forms of the jet high-energy activity, e.g. by the particle acceleration in internal shocks, is needed. The required intensity of this activity is much smaller than the final high-energy output.

(iv) The presence of a sharp boundary of the jet, with the depth of the transition layer less than a few per cent of the jet radius (which is still several orders of magnitude larger than that required for the charged particle acceleration). If the jet does not have a sharp boundary, then the formation of a supercritical regime is still possible at large distances, where the photon–photon pair production opacity declines.

ACKNOWLEDGMENTS

This work is supported by the Russian Foundation for Basic Research grant 04-02-16987, the Jenny and Antti Wihuri Foundation, the Vilho, Yrjö and Kalle Väisälä Foundation and the Academy of Finland grants 107943 and 102181.

REFERENCES

Achterberg A., Gallant Y. A., Kirk J. G., Guthmann A. W., 2001, MNRAS, 328, 393
Aloy M. A., Ibáñez J. M., Martí J. M., Gómez J.-L., Müller E., 1999, ApJ, 523, L125
Arav N., Begelman M. C., 1992, ApJ, 401, 125
Bednarz J., Ostrowski M., 1999, MNRAS, 310, L11
Berezhko E. G., 1990, Frictional Acceleration of Cosmic Rays. The Yakut Scientific Center, Yakutsk, preprint
Derishev E. V., Aharonian F. A., Kocharovsky V. V., Kocharovsky Vl. V., 2003, Phys. Rev. D, 68, 043003
Kazanas D., Georganopoulos M., Mastichiadis A., 2002, ApJ, 578, L15
Kirk J. G., Mastichiadis A., 1992, Nat, 360, 135
Ostrowski M., 2000, MNRAS, 312, 579
Paczyński B., Xu G., 1994, ApJ, 424, 708
Rees M. J., 1978, MNRAS, 184, P61
Rees M. J., Mészáros P., 1994, ApJ, 430, L93
Shakura N. I., Sunyaev R. A., 1973, A&A, 24, 337
Sikora M., Begelman M. C., Rees M. J., 1994, ApJ, 421, 153
Sikora M., Sol H., Begelman M. C., Madejski G. M., 1996, MNRAS, 280, 781
Stawarz L., Ostrowski M., 2002, ApJ, 578, 763
Stern B. E., 1985, Astron. Zh., 62, 529
Stern B. E., 2003, MNRAS, 345, 590
Stern B., Svensson R., 1991, in Zdziarski A., Sikora M., eds, Relativistic Hadrons in Cosmic Compact Objects. Lecture Notes in Physics Vol. 391. Springer-Verlag, Heidelberg, p. 41
Stern B. E., Begelman M. C., Sikora M., Svensson R., 1995, MNRAS, 272, 291
Svensson R., 1987, MNRAS, 227, 403
Zdziarski A. A., 1988, ApJ, 335, 786

This paper has been typeset from a TEX/LATEX file prepared by the author.